

Low-Rank Combinatorial Optimization and Statistical Learning by Spatial Photonic Ising Machine

Hiroshi Yamashita, Ken-ichi Okubo, Suguru Shimomura, Yusuke Ogura, Jun Tanida, and Hideyuki Suzuki*
Graduate School of Information Science and Technology, Osaka University, Osaka 565-0871, Japan

The spatial photonic Ising machine (SPIM) [D. Pierangeli et al., Phys. Rev. Lett. **122**, 213902 (2019)] is a promising optical architecture utilizing spatial light modulation for solving large-scale combinatorial optimization problems efficiently. The primitive version of the SPIM, however, can accommodate Ising problems with only rank-one interaction matrices. In this Letter, we propose a new computing model for the SPIM that can accommodate any Ising problem without changing its optical implementation. The proposed model is particularly efficient for Ising problems with low-rank interaction matrices, such as knapsack problems. Moreover, it acquires the learning ability of Boltzmann machines. We demonstrate that learning, classification, and sampling of the MNIST handwritten digit images are achieved efficiently using the model with low-rank interactions. Thus, the proposed model exhibits higher practical applicability to various problems of combinatorial optimization and statistical learning, without losing the scalability inherent in the SPIM architecture.

Introduction.—As the recent development of machine intelligence technologies relies largely on massive computational power for optimization and learning, there is a growing demand for high-speed, large-scale, and energy-efficient computation to deal with increasingly complex real-world problems. A possible approach to meet this demand is to adopt unconventional, problem-specific computing technologies, without relying on the conventional von Neumann architecture.

Ising machines are dedicated hardware solvers for combinatorial optimization problems formulated as Ising problems, designed to find the (approximate) ground states of the corresponding Ising models [1, 2]. Many important combinatorial optimization problems can be formulated as Ising problems [2, 3], thus leading to numerous studies [4–15] on implementing Ising machines using various physical devices and dynamics.

The spatial photonic Ising machine (SPIM) [13, 14] is a promising optical architecture utilizing spatial light modulation for solving large-scale Ising problems efficiently. The SPIM accelerates annealing computation by optically computing the Ising Hamiltonian with all-to-all interactions in constant time, independent of the number of variables. Its outstanding performance has been demonstrated for problems with more than ten thousand variables [16].

Despite its superior scalability, the primitive version of the SPIM can accommodate only a limited class of Ising problems with rank-one interaction matrices. Although subsequent studies [17, 18] multiplexed the SPIM to handle broader classes of Ising problems, the scalability becomes degraded instead. Thus, a breakthrough is still required for the SPIM to attain the applicability to various real-world problems without losing its scalability.

In this Letter, we propose a multicomponent computing model for the SPIM to circumvent the limitation and accommodate higher-rank interaction matrices without changing its optical implementation. The proposed model is capable of handling any Ising problem, and is particularly efficient for problems with low-rank interactions. We demonstrate its efficient applicability to knapsack problems by formulating them as Ising problems with rank two.

Moreover, we show that the proposed model acquires the

learning ability of Boltzmann machines [1]. With full-rank interactions, it has the expressive power equivalent to the ordinary Boltzmann machine; however, the model with low-rank interactions is efficient and can be sufficient for inferences from real-world data, as typically assumed in low-rank modeling. We demonstrate that learning, classification, and sampling of the MNIST handwritten digit images [19] are achieved efficiently with low-rank interactions. Notably, we observe that the newly derived learning rule naturally performs low-rank learning of the digit images, whereas low-rank constraints are not explicitly imposed.

Thus, we report here that the proposed model exhibits higher practical applicability to various problems of combinatorial optimization and statistical learning, without losing the scalability inherent in the SPIM architecture. Although our contribution in this Letter is the computing model that theoretically works with any existing SPIM implementation, we also present the results of proof-of-concept optical experiments.

Optical computation of Ising Hamiltonian.—The SPIM [13, 14] computes the Ising Hamiltonian optically from the phase-modulated image of an amplitude-modulated laser beam (Fig. 1). Light incident on the i th site of the spatial light modulator (SLM) with an amplitude ξ_i is phase-modulated by $\sigma_i = \exp(i\phi_i) = \pm 1$, which represents the i th Ising spin, and detected by an image sensor. In the primitive version of the SPIM, the detected image I is compared with the point-like target image I_T to obtain the Ising Hamiltonian in the following form:

$$H(\boldsymbol{\sigma}) \propto \sum_{i,j} \xi_i \xi_j \sigma_i \sigma_j = \boldsymbol{\sigma}^\top \boldsymbol{\xi} \boldsymbol{\xi}^\top \boldsymbol{\sigma}, \quad (1)$$

where $\boldsymbol{\xi} = (\xi_1, \dots, \xi_N)^\top$ and $\boldsymbol{\sigma} = (\sigma_1, \dots, \sigma_N)^\top$. Notably, the computation is performed in constant time, independent of the number of spins N , involving all-to-all interactions among the spins. However, compared with the ordinary (quadratic) Ising Hamiltonian $H(\boldsymbol{\sigma}) = -\frac{1}{2} \boldsymbol{\sigma}^\top \boldsymbol{J} \boldsymbol{\sigma}$, the interaction matrix \boldsymbol{J} is limited to the form $\boldsymbol{J} \propto \boldsymbol{\xi} \boldsymbol{\xi}^\top$. Thus, the primitive SPIM can accommodate only real symmetric matrices with rank one as the interaction matrix. The Ising spin system with this type of Hamiltonian is known as the Mattis model [20].

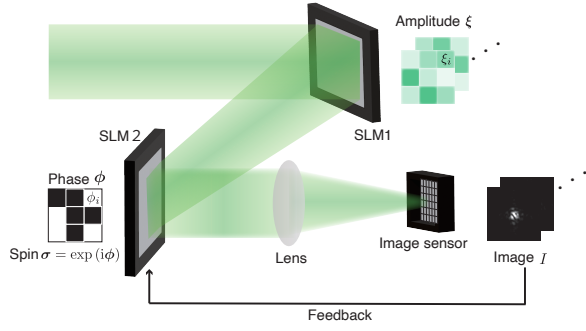


FIG. 1. Schematic of the SPIM architecture. The laser beam is amplitude-modulated and phase-modulated by spatial light modulators SLM1 and SLM2, which encode ξ and σ , respectively, and detected by an image sensor. The Ising Hamiltonian is obtained from the detected image I .

Here we propose a multicomponent computing model for the SPIM architecture to improve the expressive power of the interaction matrix. We formulate the Hamiltonian as a linear combination of Eq. (1) as follows:

$$H(\sigma) = -\frac{1}{2} \sum_{k=1}^K \lambda_k \sum_{i,j} \xi_{i,k} \xi_{j,k} \sigma_i \sigma_j = -\frac{1}{2} \sigma^\top \left(\sum_{k=1}^K \lambda_k \xi_k \xi_k^\top \right) \sigma, \quad (2)$$

where K denotes the number of components, and λ_k and $\xi_k = (\xi_{1,k}, \dots, \xi_{N,k})^\top$ are the weight and amplitude parameters of the k th component, respectively. The energy value of the Hamiltonian can be obtained by calculating the weighted sum from images acquired K times with different amplitudes ξ_k . Now the interaction matrix $J = \sum_k \lambda_k \xi_k \xi_k^\top$ can represent any real symmetric matrix with rank not greater than K . Therefore, if K is increased to N , any Ising Hamiltonian can be computed. Although the computation time increases linearly to K , it does not depend directly on N , inheriting the scalability of the underlying SPIM architecture.

Combinatorial optimization with the multicomponent model.—To solve a combinatorial optimization problem using an Ising machine, we formulate it as an Ising problem, which is to find $\sigma \in \{+1, -1\}^N$ that minimizes the Ising Hamiltonian $H(\sigma) = -\frac{1}{2} \sigma^\top J \sigma$. For simplicity, the linear (bias) term is omitted here because introducing an additional spin fixed to +1 suffices.

The Hamiltonian of the primitive SPIM, with rank $K = 1$, is $H(\sigma) = -\frac{\lambda}{2} (\xi^\top \sigma)^2$. When $\lambda > 0$, it has trivial, two symmetric global minima $\sigma = \pm \text{sgn } \xi$. When $\lambda < 0$, minimizing $H(\sigma)$ reduces to a number partitioning problem [16, 21–25], which is to find the partition of numbers ξ_1, \dots, ξ_N into two subsets that minimizes the difference of the sums in the two subsets $|\sum_i \xi_i \sigma_i| = |\xi^\top \sigma|$. Thus, the primitive SPIM can essentially handle only the class of number partitioning problems. Although this class is theoretically NP-hard [26], it is practically insufficient to be used for solving Ising formulations of various combinatorial optimization problems.

However, we can circumvent the limitation without chang-

ing the optical implementation by introducing the proposed multicomponent model, which is capable of handling any Ising problem. Particularly, it is efficient for Ising problems with low-rank interactions because the computation time depends linearly on rank K .

The spin configuration σ is updated according to energy values $H(\sigma)$. To solve an Ising problem, typically we employ simulated annealing [27]; a sample sequence of σ , generated by a Markov-chain Monte Carlo (MCMC) method from the Gibbs distribution $P(\sigma) \propto \exp[-H(\sigma)/T]$, is expected to converge to an approximate ground state as the system temperature T gradually decreases.

Application to knapsack problems.—To demonstrate the applicability of the multicomponent model to a broader class of combinatorial optimization problems, we apply it to the 0-1 knapsack problem with integer weights, which can be formulated as Ising problems with rank $K = 2$ and hence cannot be handled by the primitive SPIM.

The knapsack problem is a well-known problem to find the subset of given items that maximizes the total value satisfying a predefined total weight limit. More specifically, given the value v_i and the weight w_i of the i th item for $i = 1, 2, \dots, n$ and the weight limit W , the 0-1 knapsack problem is expressed as follows:

$$\text{maximize} \quad \sum_{i=1}^n v_i x_i \quad (3)$$

$$\text{subject to} \quad \sum_{i=1}^n w_i x_i \leq W, \quad \mathbf{x} = (x_1, \dots, x_n) \in \{0, 1\}^n. \quad (4)$$

Under the assumption of integer weights, the knapsack problem reduces to minimizing

$$H(\mathbf{x}, \mathbf{y}) = A \left(\sum_{i=1}^n w_i x_i + \sum_{i=1}^m 2^{i-1} y_i - W \right)^2 - B \left(\sum_{i=1}^n v_i x_i \right)^2, \quad (5)$$

where auxiliary variables $\mathbf{y} = (y_1, \dots, y_m) \in \{0, 1\}^m$ are introduced using a log trick [3]. This can be rewritten in the multicomponent form (2) with size $N = n + m + 1$ and rank $K = 2$ as follows:

$$\lambda_1 = -\frac{A}{2}, \quad \lambda_2 = +\frac{B}{2}, \quad (6)$$

$$\xi_1 = (w_1, \dots, w_n, 2^0, \dots, 2^{m-1}, \sum_i w_i + 2^m - 1 - 2W)^\top, \quad (7)$$

$$\xi_2 = (v_1, \dots, v_n, 0, \dots, 0, \sum_i v_i)^\top, \quad (8)$$

$$\sigma = (2x_1 - 1, \dots, 2x_n - 1, 2y_1 - 1, \dots, 2y_m - 1, 1)^\top. \quad (9)$$

We conducted a proof-of-concept experiment [28] for a knapsack problem with $n = 13$ items [29]. The spin sequences were sampled both optically and numerically at a moderately low, constant temperature. Fig. 2 shows that the multicomponent SPIM generates samples essentially according to the Gibbs distribution. The typical time evolution of the energy values $H(\sigma)$ of spins observed in the optical experiment (Fig. 2(a)) resembles that of the numerical experiment

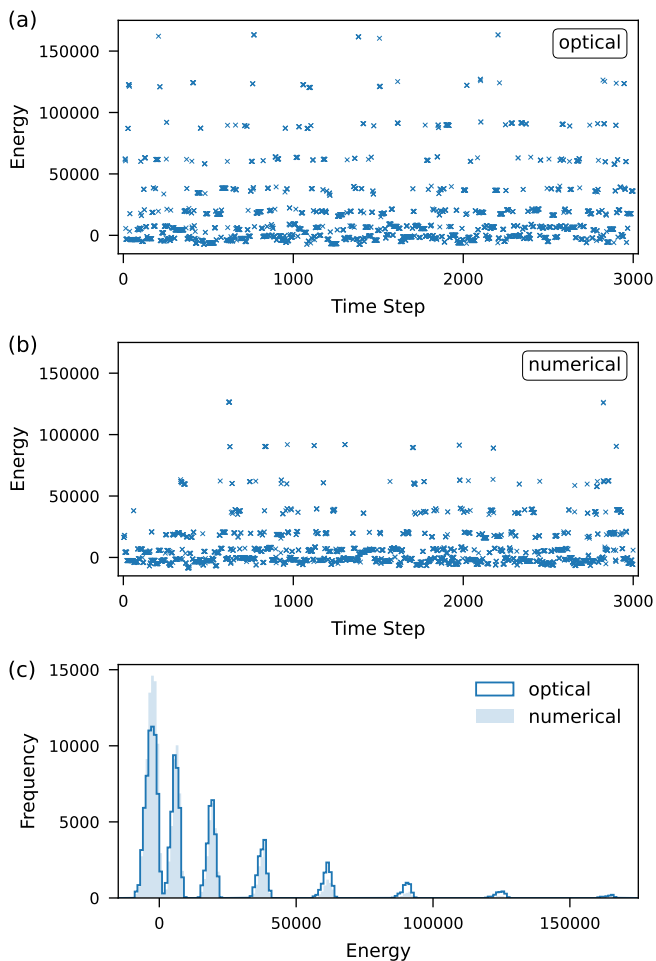


FIG. 2. Sampling behavior of the multicomponent model for a knapsack problem. Typical time evolutions of energy values of the spin configurations sampled from (a) optical and (b) numerical experiments. Several samples with higher energy values are not shown. (c) Histograms of the energy values of 3000×50 samples observed from each experiment with bin width 1000.

(Fig. 2(b)). The histogram of energy values sampled from the optical experiment (Fig. 2(c)) shows that it generates many low-energy samples around $H(\sigma) \approx 0$, constituting the distribution with peaks at the same values as those in the numerical experiment.

A closer look at these results indicates that the temperature of the Gibbs distribution was slightly higher in the optical experiment due to the noise in the optical system. Although the physical noise can be utilized as a source of randomness [30], we simply executed the Metropolis algorithm adhering to the obtained Hamiltonian values for clarity of results. To facilitate the MCMC process to jump over energy barriers, multiple-spin flips were performed, taking the advantage of direct energy computation of the SPIM.

The optimal solution to the knapsack problem was obtained 304 times out of the 150000 samples observed in the optical experiment, with a ratio considerably higher than the proba-

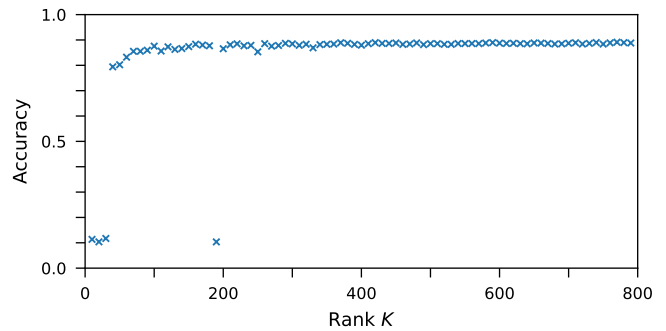


FIG. 3. Classification of MNIST digit images. The classification accuracy of the trained multicomponent models with rank K taking on integer multiples of 10 is shown.

bility 2^{-13} of random sampling. This result confirms that the spin states with lower energy values were sampled frequently according to the Gibbs distribution $P(\sigma) \propto \exp[-H(\sigma)/T]$.

Overall, we demonstrated that the multicomponent model with rank $K = 2$ works as expected with the Ising Hamiltonian for the knapsack problem in both the numerical and optical experiments. These results indicate that the proposed model can efficiently handle Ising problems with low-rank interactions.

Statistical learning with the multicomponent model.—In the field of machine learning, the Ising model is commonly referred to as the Boltzmann machine, which can be viewed as a generative neural network model composed of stochastic elements [31]. It has been applied not only for solving combinatorial optimization problems [2] but also, more importantly, for statistical machine learning. The restricted Boltzmann machine (RBM) [32–34] and deep Boltzmann machine (DBM) [35, 36] are well-known subclasses that have contributed to the recent development of deep learning.

With the increased expressive power, the multicomponent model acquires the learning ability applicable to real-world data. If rank K is increased to N , it becomes equivalent to the ordinary Boltzmann machine; however, it is efficient with low-rank interactions both in terms of the computation time and the number of parameters.

To train the model $P(\sigma) \propto \exp[-H(\sigma)]$, we perform the gradient ascent on the log-likelihood $\log L$ given the data distribution, according to the gradients [28]

$$\frac{\partial}{\partial \lambda_k} \log L = \frac{1}{2} \xi_k^T \left(\langle \sigma \sigma^T \rangle_{\text{data}} - \langle \sigma \sigma^T \rangle_{\text{model}} \right) \xi_k, \quad (10)$$

$$\frac{\partial}{\partial \xi_k} \log L = \lambda_k \left(\langle \sigma \sigma^T \rangle_{\text{data}} - \langle \sigma \sigma^T \rangle_{\text{model}} \right) \xi_k, \quad (11)$$

where $\langle \cdot \rangle_{\text{data}}$ and $\langle \cdot \rangle_{\text{model}}$ denote the expectations over the data and model distributions, respectively.

Learning MNIST digit images.—To demonstrate the learning ability as a Boltzmann machine with the low-rank efficiency, we trained the multicomponent model [28] using the MNIST digit image data [19].

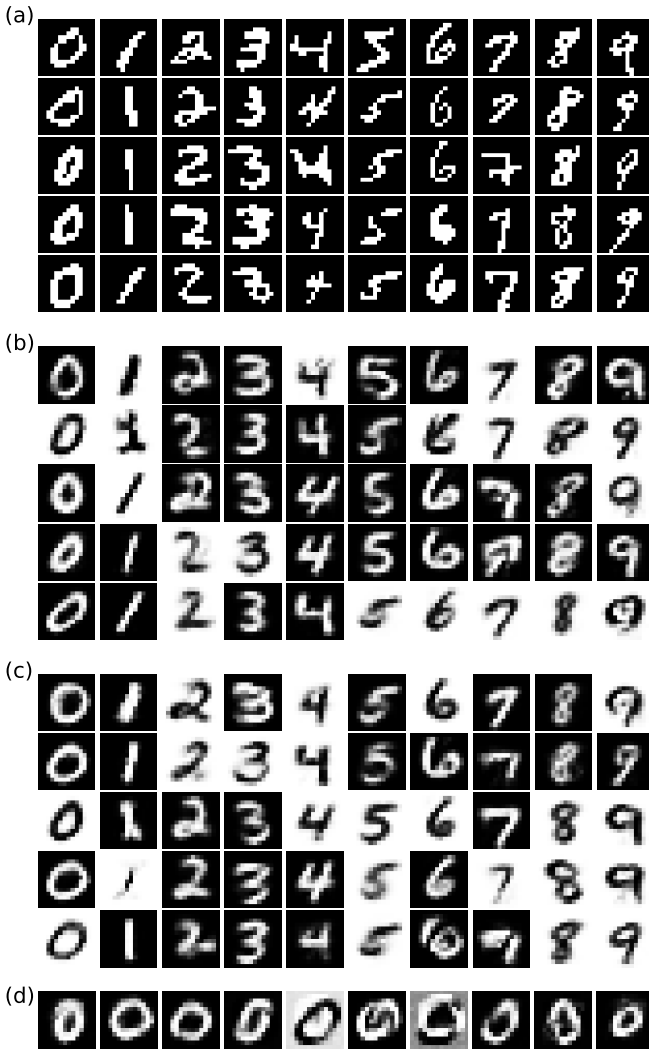


FIG. 4. Sampling from the multicomponent models trained with the MNIST digit images. (a) Random samples from the training dataset. Random samples generated from (b) the trained models with rank $K = 50$, (c) the reduced models with only principal components, and (d) the optical experiment of the reduced model, after 1960 time steps from random initial spin configurations. Each pixel in the gray-scale images represents the conditional probability $P[\sigma_i = 1 | \sigma_{\setminus i}]$ of each spin σ_i given the states of other spins $\sigma_{\setminus i}$.

First, we applied it for the classification of handwritten digits to evaluate its low-rank efficiency. We trained the fully visible model with size $N = 794$. Fig. 3 shows the dependency of the classification accuracy on rank K . Although the accuracy drops to the chance level for $K \leq 30$ owing to training failure, the graph is almost flat for $K \geq 100$; that is, the model with rank as low as $K = 100$ exhibits a performance comparable to that of the full rank. This numerical result clearly shows the low-rank efficiency of the multicomponent model in learning the MNIST images. Note that the accuracy was not as high as that of the ordinary RBM due to the lack of hidden units.

Next, we sampled digit images from the fully visible multicomponent models with size $N = 196$ and rank $K = 50$ trained

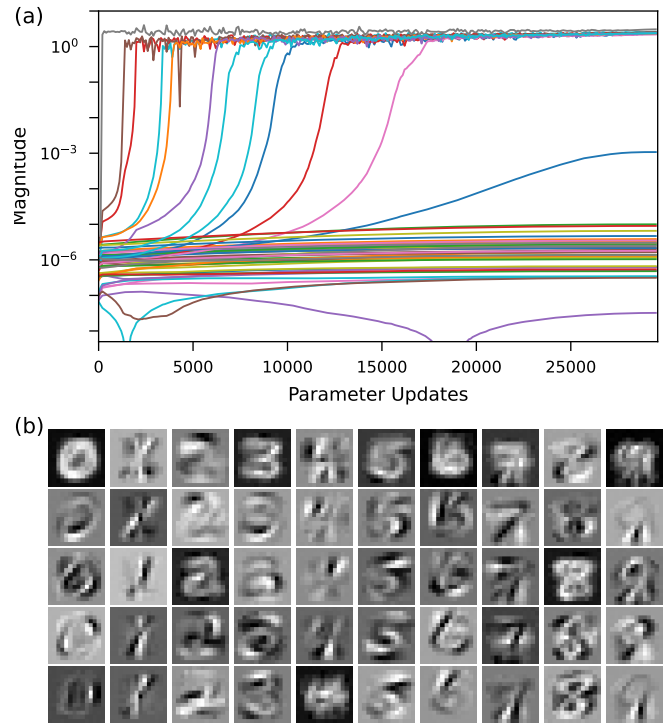


FIG. 5. Low-rank learning of the multicomponent model. (a) Time evolution of the magnitude values $|\lambda_k| \|\xi_k\|^2$ in the learning process of the model with rank $K = 50$ for the digit “0”. (b) Gray-scale images of principal components ξ_k with the five largest magnitude values for each digit.

using the MNIST images of each digit (Fig. 4(a)). Random samples from the trained models (Fig. 4(b)) show that the digit images were successfully sampled. Note that inverse images are sampled due to the symmetry $H(\sigma) = H(-\sigma)$ of the model without bias. The images did not degrade in random samples from the reduced model (Fig. 4(c)) composed only of principal components with magnitudes $|\lambda_k| \|\xi_k\|^2 > 0.1$. These numerical results indicate that the reduced, low-rank model is sufficient for sampling. Fig. 4(d) shows random samples obtained optically from the reduced model for the digit “0”. Some samples maintain the digit shape, while some appear to degrade, in comparison with the numerical results, possibly due to the noise in the optical system. Again, we did not utilize the physical noise for clarity of results.

The learning behavior for the digit “0” is depicted in Fig. 5(a). The magnitude $|\lambda_k| \|\xi_k\|^2$ for each k th component increases one by one as the learning process progresses. The final number of principal components is 11 out of $K = 50$. The multicomponent model appears to gradually increase its (effective) rank as required for accuracy. This result suggests that the gradient-ascent learning rule naturally achieves low-rank learning. Fig. 5(b) shows the gray-scale images of the top five principal components ξ_k , for which λ_k is positive. The digit shapes are vaguely embedded in ξ_k , because intuitively, $\sigma = \pm \text{sgn} \xi_k$ minimizes the k th component if $\lambda_k > 0$.

Overall, both the classification and sampling results demonstrate the low-rank efficiency of the multicomponent model in learning MNIST digit images with the gradient-ascent learning rule.

Discussion.—Since the multicomponent model handles lower-rank Ising problems more efficiently, the matrix ranks can be an index that characterizes a new aspect, to the best of our knowledge, for combinatorial optimization problems. The number partitioning problem and the 0-1 knapsack problem with integer weights are lowest-rank examples of combinatorial optimization problems. It is an interesting future direction to characterize the types of low-rank real-world problems.

The efficiency for low-rank Ising Hamiltonians as well as inherent scalability with all-to-all interactions is a unique feature that cannot be seen in other Ising machines. For rank one, its outstanding performance has already been demonstrated in solving large-scale number partitioning problems [16]. Thus, the multicomponent SPIM is also expected to exhibit unique performance for large-scale Ising problems with low-rank all-to-all interactions.

A necessity for solving low-rank Ising problems arises when the learning is involved [37–39]. For example, a study on the automated design of metamaterials [37] trains a factorization machine [40], similar to the multicomponent model, to find low-energy candidates for metamaterials using a D-Wave quantum annealer. Here, the low-rank constraint contributes to the generalization ability, which is essential for inferring the energy landscape only from a small dataset. Thus, the multicomponent SPIM should serve as an efficient sampling machine to find low-energy candidates using a trained low-rank Ising Hamiltonian.

Despite the importance of low-rank modeling in data science, there has been no study on low-rank learning of Boltzmann machines, to the best of our knowledge. Our results suggest the capabilities of the low-rank Boltzmann machine as a statistical model with high parameter efficiency. The low-rank learning may be further enhanced by introducing sparsity regularization. Elucidating the mechanism behind the gradient-ascent rule is also intriguing.

Another unique feature of the multicomponent SPIM is that we can choose candidate states arbitrarily in MCMC algorithms without any loss of the computation speed, as demonstrated in multiple-spin flips for the knapsack problem. Designing new MCMC algorithms specialized for the multicomponent SPIM is considered important, possibly by exploiting the low-rank property [41] and physical noise [30].

The high practical applicability of the multicomponent SPIM highlights the need for hardware improvements in the SPIM, such as enhanced computation speed and scalability, for further development. It can exploit the low-rank property in multiplexed architectures such as [18]. If the SPIM hardware allows σ to take nonbinary, intermediate continuous values, we can implement continuous-valued spin systems with rich nonlinear dynamics as in Refs. [7–9, 42–48].

In conclusion, we proposed the multicomponent computing model for the SPIM that exhibits higher practical applicability

to various problems of combinatorial optimization and statistical learning without losing the inherent scalability. Notably, the proposed model has a unique affinity to low-rank combinatorial optimization and low-rank learning of Boltzmann machines. These unexpected benefits of the SPIM architecture are expected to contribute to the future development of non-von Neumann, neuro-inspired computing.

This study was supported by JST CREST JPMJCR18K2. H.Y. and H.S. appreciate the support from JST Moonshot R&D JPMJMS2021 and the WPI-IRCn at UTIAS.

H.Y. and K.O. contributed equally to this work.

* hideyuki@ist.osaka-u.ac.jp

- [1] D. H. Ackley, G. E. Hinton, and T. J. Sejnowski, A learning algorithm for Boltzmann machines, *Cogn. Sci.* **9**, 147 (1985).
- [2] J. H. Korst and E. H. Aarts, Combinatorial optimization on a Boltzmann machine, *J. Parallel Distrib. Comput.* **6**, 331 (1989).
- [3] A. Lucas, Ising formulations of many NP problems, *Front. Phys.* **2**, 10.3389/fphy.2014.00005 (2014).
- [4] N. Mohseni, P. L. McMahon, and T. Byrnes, Ising machines as hardware solvers of combinatorial optimization problems, *Nat. Rev. Phys.* **4**, 363–379 (2022).
- [5] M. W. Johnson, M. H. S. Amin, S. Gildert, T. Lanting, F. Hamze, N. Dickson, R. Harris, A. J. Berkley, J. Johansson, P. Bunyk, E. M. Chapple, C. Enderud, J. P. Hilton, K. Karimi, E. Ladizinsky, N. Ladizinsky, T. Oh, I. Perminov, C. Rich, M. C. Thom, E. Tolkacheva, C. J. S. Truncik, S. Uchaikin, J. Wang, B. Wilson, and G. Rose, Quantum annealing with manufactured spins, *Nature* **473**, 194–198 (2011).
- [6] M. Yamaoka, C. Yoshimura, M. Hayashi, T. Okuyama, H. Aoki, and H. Mizuno, A 20k-spin Ising chip to solve combinatorial optimization problems with CMOS annealing, *IEEE J. Solid-State Circuits* **51**, 303 (2016).
- [7] T. Inagaki, Y. Haribara, K. Igarashi, T. Sonobe, S. Tamate, T. Honjo, A. Marandi, P. L. McMahon, T. Umeki, K. Enbutsu, O. Tadanaga, H. Takenouchi, K. Aihara, K.-I. Kawarabayashi, K. Inoue, S. Utsunomiya, and H. Takesue, A coherent Ising machine for 2000-node optimization problems, *Science* **354**, 603–606 (2016).
- [8] T. Leleu, Y. Yamamoto, P. L. McMahon, and K. Aihara, Destabilization of local minima in analog spin systems by correction of amplitude heterogeneity, *Phys. Rev. Lett.* **122**, 040607 (2019).
- [9] H. Goto, K. Tatsumura, and A. R. Dixon, Combinatorial optimization by simulating adiabatic bifurcations in nonlinear Hamiltonian systems, *Sci. Adv.* **5**, eaav2372 (2019).
- [10] S. Tsukamoto, M. Takatsu, S. Matsubara, and H. Tamura, An accelerator architecture for combinatorial optimization problems., *Fujitsu Sci. Tech. J.* **53**, 8–13 (2017).
- [11] T. Okuyama, T. Sonobe, K.-I. Kawarabayashi, and M. Yamaoka, Binary optimization by momentum annealing, *Phys. Rev. E* **100**, 012111 (2019).
- [12] T. Wang and J. Roychowdhury, OIM: Oscillator-based Ising machines for solving combinatorial optimisation problems, in *Unconventional Computation and Natural Computation (UCNC 2019)*, edited by I. McQuillan and S. Seki (2019) pp. 232–256.
- [13] D. Pierangeli, G. Marcucci, and C. Conti, Large-scale photonic Ising machine by spatial light modulation, *Phys. Rev. Lett.* **122**,

- 213902 (2019).
- [14] D. Pierangeli, G. Marcucci, and C. Conti, Adiabatic evolution on a spatial-photonic Ising machine, *Optica* **7**, 1535 (2020).
- [15] F. Böhm, D. Alonso-Urquijo, G. Verschaffelt, and G. Van der Sande, Noise-injected analog Ising machines enable ultrafast statistical sampling and machine learning, *Nat. Commun.* **13**, 5847 (2022).
- [16] A. Prabhakar, P. Shah, U. Gautham, V. Natarajan, V. Ramesh, N. Chandrachoodan, and S. Tayur, Optimization with photonic wave-based annealers, *Phil. Trans. R. Soc. A.* **381**, 20210409 (2023).
- [17] W. Sun, W. Zhang, Y. Liu, Q. Liu, and Z. He, Quadrature photonic spatial Ising machine, *Opt. Lett.* **47**, 1498 (2022).
- [18] L. Luo, Z. Mi, J. Huang, and Z. Ruan, Wavelength-division multiplexing optical Ising simulator enabling fully programmable spin couplings and external magnetic fields (2023), arXiv:2303.11565 [physics.optics].
- [19] Y. LeCun, C. Cortes, and C. J. Burges, The MNIST database of handwritten digits, <https://yann.lecun.com/exdb/mnist/>.
- [20] D. Mattis, Solvable spin systems with random interactions, *Phys. Lett. A* **56**, 421 (1976).
- [21] F. F. Ferreira and J. F. Fontanari, Probabilistic analysis of the number partitioning problem, *J. Phys. A Math. Gen.* **31**, 3417 (1998).
- [22] S. Mertens, Phase transition in the number partitioning problem, *Phys. Rev. Lett.* **81**, 4281 (1998).
- [23] S. Mertens, A physicist's approach to number partitioning, *Theor. Comput. Sci.* **265**, 79 (2001).
- [24] D. Pierangeli, M. Rafayelyan, C. Conti, and S. Gigan, Scalable spin-glass optical simulator, *Phys. Rev. Appl.* **15**, 034087 (2021).
- [25] J. Huang, Y. Fang, and Z. Ruan, Antiferromagnetic spatial photonic Ising machine through optoelectronic correlation computing, *Commun. Phys.* **4**, 242 (2021).
- [26] J. P. Pedroso and M. Kubo, Heuristics and exact methods for number partitioning, *Eur. J. Oper. Res.* **202**, 73 (2010).
- [27] S. Kirkpatrick, C. D. Gelatt, and M. P. Vecchi, Optimization by simulated annealing, *Science* **220**, 671 (1983).
- [28] See Supplemental Material for the experimental details and derivation of the learning rule.
- [29] D. Pisinger, Core problems in knapsack algorithms, *Oper. Res.* **47**, 570 (1999).
- [30] D. Pierangeli, G. Marcucci, D. Brunner, and C. Conti, Noise-enhanced spatial-photonic Ising machine, *Nanophotonics* **9**, 4109 (2020).
- [31] I. Goodfellow, Y. Bengio, and A. Courville, *Deep Learning* (MIT Press, 2016) <http://www.deeplearningbook.org>.
- [32] P. Smolensky, Information processing in dynamical systems: Foundations of harmony theory, in *Parallel Distributed Processing: Explorations in the Microstructure of Cognition*, edited by D. E. Rumelhart and J. L. McClelland (MIT Press, Cambridge, 1986).
- [33] G. E. Hinton, Training products of experts by minimizing contrastive divergence, *Neural Comput.* **14**, 1771 (2002).
- [34] H. Larochelle and Y. Bengio, Classification using discriminative restricted Boltzmann machines, in *The 25th International Conference on Machine Learning (ICML 2008)*, edited by A. McCallum and S. Roweis (2008) p. 536–543.
- [35] R. Salakhutdinov and G. Hinton, Deep Boltzmann machines, in *The 12th International Conference on Artificial Intelligence and Statistics (AISTATS 2009)*, Proceedings of Machine Learning Research, Vol. 5, edited by D. van Dyk and M. Welling (2009) pp. 448–455.
- [36] R. Salakhutdinov and G. Hinton, An efficient learning procedure for deep Boltzmann machines, *Neural Comput.* **24**, 1967 (2012).
- [37] K. Kitai, J. Guo, S. Ju, S. Tanaka, K. Tsuda, J. Shiomi, and R. Tamura, Designing metamaterials with quantum annealing and factorization machines, *Phys. Rev. Res.* **2**, 013319 (2020).
- [38] B. A. Wilson, Z. A. Kudyshev, A. V. Kildishev, S. Kais, V. M. Shalaev, and A. Boltasseva, Machine learning framework for quantum sampling of highly constrained, continuous optimization problems, *Appl. Phys. Rev.* **8**, 041418 (2021).
- [39] T. Matsumori, M. Taki, and T. Kadowaki, Application of QUBO solver using black-box optimization to structural design for resonance avoidance, *Sci. Rep.* **12**, 12143 (2022).
- [40] S. Rendle, Factorization machines, in *IEEE International Conference on Data Mining (ICDM 2010)*, edited by G. I. Webb, B. Liu, C. Zhang, D. Gunopulos, and X. Wu (2010) pp. 995–1000.
- [41] F. Koehler, H. Lee, and A. Risteski, Sampling approximately low-rank Ising models: MCMC meets variational methods, in *The 35th Annual Conference on Learning Theory (COLT 2022)*, Proceedings of Machine Learning Research, Vol. 178, edited by P.-L. Loh and M. Raginsky (2022) pp. 4945–4988.
- [42] H. Suzuki, J. Imura, Y. Horio, and K. Aihara, Chaotic Boltzmann machines, *Sci. Rep.* **3**, 1610 (2013).
- [43] H. Suzuki, Monte Carlo simulation of classical spin models with chaotic billiards, *Phys. Rev. E* **88**, 052144 (2013).
- [44] F. L. Traversa and M. Di Ventra, Polynomial-time solution of prime factorization and NP-complete problems with digital memcomputing machines, *Chaos* **27**, 023107 (2017).
- [45] S. R. B. Bearden, Y. R. Pei, and M. Di Ventra, Efficient solution of Boolean satisfiability problems with digital memcomputing, *Sci. Rep.* **10**, 19741 (2020).
- [46] M. Ercsey-Ravasz and Z. Toroczkai, Optimization hardness as transient chaos in an analog approach to constraint satisfaction, *Nat. Phys.* **7**, 966–970 (2011).
- [47] H. Yamashita, K. Aihara, and H. Suzuki, Timescales of Boolean satisfiability solver using continuous-time dynamical system, *Commun. Nonlinear Sci. Numer. Simul.* **84**, 105183 (2020).
- [48] H. Yamashita, K. Aihara, and H. Suzuki, Accelerating numerical simulation of continuous-time Boolean satisfiability solver using discrete gradient, *Commun. Nonlinear Sci. Numer. Simul.* **102**, 105908 (2021).

Supplemental material for Low-Rank Combinatorial Optimization and Statistical Learning by Spatial Photonic Ising Machine

Hiroshi Yamashita, Ken-ichi Okubo, Suguru Shimomura,
Yusuke Ogura, Jun Tanida, and Hideyuki Suzuki*
*Graduate School of Information Science and Technology,
Osaka University, Osaka 565-0871, Japan*

I. OPTICAL SETUP FOR THE SPIM ARCHITECTURE

We implemented the SPIM architecture (Fig. 1 in the main text) for our proof-of-concept optical experiments. Light patterns with amplitudes ξ_k are generated by using SLM1 (Santec, SLM-200, pixel size 1920×1080 , pixel pitch: $8 \mu\text{m}$) and a laser with a wavelength of 532 nm. Spin configuration σ is encoded into the modulation pattern with binary phases by SLM2 (Hamamatsu Photonics, X15213-01, pixel size 1272×1024 , pixel pitch: $12.5 \mu\text{m}$). The light intensity I_k is detected by a CMOS image sensor (Point Gray Research, Grasshopper GS3-U3-32S4, pixel pitch: $3.45 \mu\text{m}$). Note that if $\xi_{i,k}$ is negative, we flip the spin σ_i and use $|\xi_{i,k}|$ as the amplitude. Finally, we obtain the Ising Hamiltonian as a weighted sum of I_k with coefficients λ_k after capturing I_k with different amplitudes ξ_k for K times.

II. EXPERIMENTS ON A KNAPSACK PROBLEM

A knapsack problem generator [29] was used to obtain the following problem instance for the proof-of-concept experiment:

$$\begin{aligned}n &= 13, & W &= 80, \\ \mathbf{v} &= (7, 7, 8, 8, 2, 7, 12, 4, 9, 14, 2, 7, 14), \\ \mathbf{w} &= (6, 7, 1, 15, 14, 8, 5, 6, 4, 7, 5, 12, 10).\end{aligned}$$

* hideyuki@ist.osaka-u.ac.jp

The optimal solution to this problem is $\mathbf{x} = (1, 1, 1, 1, 0, 1, 1, 0, 1, 1, 1, 1, 1)$, for which the total value is 95 and the total weight is 80. The coefficients of the Ising formulation are $A = 2633$ and $B = 1$. The number of auxiliary variables is $m = 4$.

Note that the number of auxiliary variables for log trick is generally set as $m = \lceil \log_2 W \rceil + 1$; however, in this study, we set $m = \lceil \log_2 \max_i w_i \rceil$, assuming that the problem is nontrivial, $\sum_i w_i > W$. Coefficient A for the constraint term has to be sufficiently large compared with B for the total value term because the constraint violation should be penalized more than the gain of picking an item; specifically, we set $A = v_{\max} (2 \sum_i v_i - v_{\max}) + 1$ and $B = 1$, where $v_{\max} = \max_i v_i$.

In each of the optical experiment and numerical experiment, we generated 50 sample sequences of length 3000 using the Metropolis algorithm on the Gibbs distribution $P(\boldsymbol{\sigma}) \propto \exp[-H(\boldsymbol{\sigma})/T]$ at a constant temperature $T = 10A$ for random initial spin configurations. In each time step, a candidate state $\boldsymbol{\sigma}'$ is generated by flipping the spins of the current state $\boldsymbol{\sigma}$ with a probability $3/(n + m)$ for each spin, except for the last one fixed to $\sigma_N = +1$.

III. EXPERIMENTS ON MNIST DIGIT IMAGE DATA

For classification of handwritten digits, we prepared fully visible multicomponent models of size $N = 794$, composed of 784 units for 28×28 pixels of MNIST digit images and 10 units for the one-hot encoding of the 10 digit classes. We set the rank K of the models to integer multiples of 10 in the range $10 \leq K \leq 790$ and trained each of them using the 60000 MNIST training images. To obtain the model expectation in the learning rule, we used the contrastive divergence (CD) algorithm [33]. We monitored the pseudo-likelihood and stopped training before the learning degraded. The hyperparameter values are common to all the rank values: the initial learning rates, 10^{-3} and 10^{-5} for λ_k and ξ_k , respectively; the regularization coefficient, 0.001 for both λ_k and ξ_k . Classification was performed by selecting the digit whose corresponding one-hot vector minimizes the Hamiltonian with the given image data. The classification accuracy was quantified as the ratio of the number of images classified accurately out of the 10000 MNIST test images.

For sampling digit images, we prepared 10 fully visible multicomponent models with size $N = 196$ and rank $K = 50$. We trained them using the MNIST training image data of each digit, in which the digit images were shrunk to 14×14 pixels and binarized. To obtain the model expectation in the learning rule, we used the persistent contrastive divergence (PCD) algorithm [36] with 100 persistent chains. The hyperparameter values are common to all digits: the initial

learning rates, 10^{-2} and 0.5×10^{-3} for λ_k and ξ_k , respectively; the regularization coefficient, 0.001 for both λ_k and ξ_k . The reduced model was composed using only principal components with magnitudes $|\lambda_k| \|\xi_k\|^2 > 0.1$. Digit images were sampled by executing the Metropolis algorithm on each model for 1960 time steps with candidates generated by sequential single-spin flips starting from random initial spin configurations.

IV. LEARNING RULE FOR THE MULTICOMPONENT MODEL

The learning rule for the multicomponent model is derived as the gradient-ascent algorithm on the log-likelihood, adopting the same approach as the ordinary Boltzmann machine.

For the model distribution with multicomponent Hamiltonian $H(\sigma)$,

$$P(\sigma) = \frac{1}{Z} \exp[-H(\sigma)], \quad Z = \sum_{\sigma} \exp[-H(\sigma)], \quad (\text{S1})$$

the log-likelihood $\log L$ for a data distribution is given as follows:

$$\log L = \langle \log P(\sigma) \rangle_{\text{data}} = -\langle H(\sigma) \rangle_{\text{data}} - \log Z. \quad (\text{S2})$$

Using the derivatives of $\log Z$ with respect to the model parameters,

$$\frac{\partial}{\partial \lambda_k} \log Z = \frac{1}{Z} \sum_{\sigma} \frac{\partial}{\partial \lambda_k} \exp[-H(\sigma)] = -\left\langle \frac{\partial H}{\partial \lambda_k} \right\rangle_{\text{model}}, \quad (\text{S3})$$

$$\frac{\partial}{\partial \xi_k} \log Z = \frac{1}{Z} \sum_{\sigma} \frac{\partial}{\partial \xi_k} \exp[-H(\sigma)] = -\left\langle \frac{\partial H}{\partial \xi_k} \right\rangle_{\text{model}}, \quad (\text{S4})$$

we obtain the derivatives of the log-likelihood as follows:

$$\frac{\partial}{\partial \lambda_k} \log L = -\left\langle \frac{\partial H}{\partial \lambda_k} \right\rangle_{\text{data}} + \left\langle \frac{\partial H}{\partial \lambda_k} \right\rangle_{\text{model}}, \quad (\text{S5})$$

$$\frac{\partial}{\partial \xi_k} \log L = -\left\langle \frac{\partial H}{\partial \xi_k} \right\rangle_{\text{data}} + \left\langle \frac{\partial H}{\partial \xi_k} \right\rangle_{\text{model}}, \quad (\text{S6})$$

which are identical to Eqs. (10) and (11) in the main text as the multicomponent Hamiltonian

$$H(\sigma) = -\frac{1}{2} \sum_k \lambda_k (\xi_k^\top \sigma)^2, \quad (\text{S7})$$

has the following derivatives:

$$\frac{\partial H}{\partial \lambda_k} = -\frac{1}{2} \frac{\partial}{\partial \lambda_k} \sum_{k'} \lambda_{k'} (\xi_{k'}^\top \sigma)^2 = -\frac{1}{2} \xi_k^\top \sigma \sigma^\top \xi_k, \quad (\text{S8})$$

$$\frac{\partial H}{\partial \xi_k} = -\frac{1}{2} \frac{\partial}{\partial \xi_k} \sum_{k'} \lambda_{k'} (\xi_{k'}^\top \sigma)^2 = -\lambda_k \sigma \sigma^\top \xi_k. \quad (\text{S9})$$

We can introduce regularization in the learning process to avoid overfitting. We use the L2 regularizer on the parameters λ_k and ξ_k in this study.